ACS Sustainable Chemistry & Engineering

pubs.acs.org/journal/ascecg

Research Article

CO_2 Photoreduction with CuO NPs Supported by TiO_2 and $BaTiO_3$ Photoactive Materials: An *Operando* AP-NEXAFS Study

Giulia Forghieri, Silvia Mauri,* Sara Stolfi, Elena Ghedini, Elizaveta Kozyr, Lorenzo Mino, Piero Torelli, and Michela Signoretto

Cite This: https://doi.org/10.1021/acssuschemeng.5c06087

Read Online

ACCESS | Metrics & More | Article Recommendations | Supporting Information

ABSTRACT: Using light and water vapor to reduce CO_2 into various carbon-based products, such as methane, is a promising strategy to achieve the conversion of CO_2 into useful products. Copper (Cu) is a well-studied photocatalyst due to its high affinity for carbon intermediates, favoring the CO_2 evolution reaction (CER) over the hydrogen evolution reaction (HER). Recently, we have shown that adding CuO nanoparticles to light-sensitive materials such as $BaTiO_3$ (BTO) and TiO_2 enhances the photocatalytic performance of the materials. Therefore, to elucidate the interaction between CuO nanoparticles and support materials, we combined the results of standard (scanning electron microscopy, X-ray photoemission spectroscopy) and advanced characterization techniques, namely, *operando* ambient-pressure near-edge X-ray absorption fine structure (NEXAFS) and *in situ* Fourier transform infrared (FTIR) spectroscopies, for investigating the photocatalytic reaction mechanism of CuO−BTO and CuO−TiO_2 photocatalysts in *operando* CO_2 photoreduction conditions. Our results confirmed enhanced methanation on the CuO−BTO system over a TiO_2-based catalyst: NEXAFS analysis allowed to establish that the activity of both catalysts is linked to the formation of a reversible redox couple Cu^+/Cu^{2+} and that the CuO−BTO interface can promote a more efficient charge separation; the electron trapping on Ti centers was directly observed on Ti NEXAFS spectra, evidencing a strong charge recombination suppression, which can favor CO_2 reduction. IR revealed that CO_2 is strongly activated on the CuO−BTO surface, forming carbonates that are converted to CH_4 through the formation of formates as intermediates.

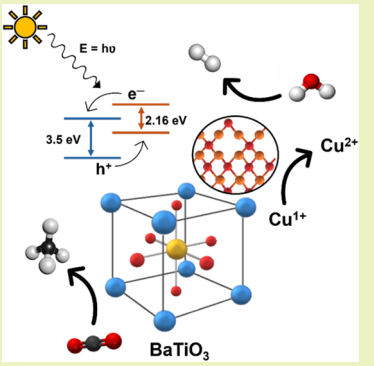

KEYWORDS: *photocatalysis, CO_2 evolution reaction, operando spectroscopy, photofuels, perovskites*

INTRODUCTION

As carbon dioxide (CO_2) levels rise—being among the major contributors to the average temperature increase globally—so does the need to modulate its concentration in the atmosphere to alleviate the global-warming-related impact.[1] Among the various available strategies, the development of technologies for the efficient capture and conversion of CO_2 is particularly promising, as they allow both for its removal and transformation into useful products, thus closing the carbon cycle. Despite being appealing, carbon capture and storage (CCS) technologies are still energy-intensive and can require up to 40% of the energy relative to the entire process.[2] On the other hand, coupling capture technologies with consequent CO_2 utilization (CCU) can improve the uptake efficiency by considerably reducing the overall CO_2 emissions.[3] In this context, by achieving the conversion of CO_2 into various C-based products by using light as the energy source and water vapor as the proton source, photocatalysis emerged as an appealing strategy to further abate the energy requirements of the overall process.[4]

Copper (Cu) has been extensively studied as both photo- and photoelectrocatalysts, for its high affinity with C-intermediates, thus more easily leading to CO_2 over the H_2O evolution reaction.[5] The coupling of copper oxide nanoparticles (CuO NPs) to other photocatalysts showed enhanced performance in CO_2 photoreduction.[6] On the other hand, perovskite materials are progressively emerging as promising photocatalysts for light-driven reduction of CO_2. In fact, the unique and tunable crystal structure of perovskites makes them adaptable to various applications, enabling the modulation of properties like light absorption, charge separation, and catalytic activity.[7] Among other perovskites, barium titanate ($BaTiO_3$), a nontoxic material based on abundant elements, has been applied to various photocatalytic processes such as the degradation of pollutants, water depuration, hydrogen production, and, only recently, CO_2 photoreduction.[7−9] A previous study has shown that the addition of CuO to $BaTiO_3$ greatly increases the selectivity toward CH_4 and the performance of $BaTiO_3$ as a catalyst.[10] However, the origin of this

Received: June 20, 2025
Revised: April 1, 2026
Accepted: April 2, 2026

effect and the underlying mechanisms of CO_2 conversion into methane at the semiconductor interface remain to be elucidated. In fact, various studies revealed that CuO can act both as a catalyst and as a reactant during the photocatalytic process.[11,12] Besides morphology and dimension, it was observed that the Cu oxidation state can considerably influence the catalyst's stability and performance.[13] Although it was observed that both Cu^0 and Cu^{1+} can act as active sites for CO_2 reduction,[14] the presence of mixed Cu^{1+} and Cu^{2+} states is usually observed during the reaction.[15] Therefore, the final photocatalytic performance also depends on the ability of the support to reduce Cu^{2+} and stabilize the active form of the Cu catalyst. Consequently, it is possible that different materials used as both CuO NPs supports and cocatalysts can differently affect the oxidation state of Cu and thus the resulting photocatalytic performance.

Near-edge X-ray absorption fine structure (NEXAFS) spectroscopy is a powerful tool to elucidate the electronic structure of various materials. It is particularly useful when employed in the soft X-ray regime for the study of first-row transition metals, since the related NEXAFS L edges are particularly sensitive to the local geometry and the oxidation state of the absorbing atom.[16] In this study, the soft X-ray NEXAFS technique has been applied in *operando* conditions, i.e., the spectra have been acquired at the real operating conditions of the photocatalyst. In this way, the electronic structure and local chemical environment modifications of the chemical species of the catalysts have been monitored in real time during the photocatalytic reaction, with a simultaneous collection of the reaction products.[17,18]

The aim of this study was to elucidate the redox behavior of CuO NPs in the prepared Cu-based materials and therefore to reveal the role of the catalysts in the presence of reagents and UV light, as to mimic the standard reaction conditions during CO_2 photoreduction. To this end, previously prepared CuO−$BaTiO_3$ and CuO−TiO_2 photocatalysts[10] were studied via *operando* ambient-pressure NEXAFS[19] to gain insights into the redox behavior and thus identify the active phases involved in the reaction. Understanding the interaction between CuO nanoparticles and perovskite materials is key to optimizing these photocatalytic systems and potentially increasing the efficiency of the photocatalytic conversion of CO_2. Results gave clues on the role of the different semiconductor species and revealed that the presence of a support-dependent effect can influence the redox state of Cu NPs and therefore the resulting catalytic performance.

RESULTS AND DISCUSSION

The Ba-based sample analyzed in this work was prepared by hydrothermal synthesis, while commercial P25 was used as the TiO_2 benchmark, as described in the Experimental Methods section. Physisorption analysis of the synthesized catalysts revealed a mesoporous structure, with a higher BET surface area of $BaTiO_3$ (149 $m^2\ g^{-1}$) compared to that of TiO_2 (50 $m^2\ g^{-1}$). The addition of CuO NPs did not considerably affect the surface area of the samples, as reported in Table 1. Despite having different surface areas, SEM analysis of TiO_2 and $BaTiO_3$ samples showed irregularly shaped particles of similar average dimensions (Figure 1a,b), showing particle size average distributions of 21.4 ± 4.1 nm and 29.9 ± 8.6 nm, respectively (Figure 1c,d). The $BaTiO_3$-based samples showed a higher average pore size compared to the TiO_2 samples (Table 1). For both samples, the addition of CuO NPs

Table 1. BET Surface Area, Average Pore Sizes, and Pore Volumes Calculated for all Samples after N_2 Physisorption Analysis

sample	BET ($m^2\ g^{-1}$)	average pore size (nm)	pore volume (cm^3/g)
$BaTiO_3$	149	8.4	0.03
TiO_2	50	6.5	0.08
CuO−$BaTiO_3$	137	13.6	0.4
CuO−TiO_2	49	8	0.1

increased the average pore size while slightly decreasing the BET surface area to 137 $m^2\ g^{-1}$ and 49 $m^2\ g^{-1}$ for CuO−$BaTiO_3$ and CuO−TiO_2, respectively. SEM and SEM-EDS analyses combined with HRTEM and SAED characterization on the Cu−$BaTiO_3$ and Cu−TiO_2 materials had been previously conducted,[10] confirming the nanostructured morphology of CuO NPs, appearing as aggregates of roughly 200 nm constituted by smaller spherical nanoparticles (d < 10 nm), homogeneously distributed on the surface of both $BaTiO_3$ and TiO_2 samples.

XPS analysis was performed on the pristine samples, showing the expected elemental composition without a trace of significant contaminants. The 2p core level of Cu and Ti XPS spectra of $BaTiO_3$, CuO−$BaTiO_3$, and CuO−TiO_2 are reported in Figure 2a,b. Although the predominant oxidation state detected in all three samples was Ti^{4+}, a small presence of Ti^{3+} and Ti^{2+} states was also observed in both $BaTiO_3$ and CuO−$BaTiO_3$ (Figure 2a). The presence of oxidation states different from +4 can be attributed to the amorphous portions detected within the $BaTiO_3$ materials, as well as to the possible presence of surface defects such as oxygen vacancies and under-coordinated surface atoms, as also suggested by previous XRD and TEM analysis showing structural irregularities potentially influencing the titanium oxidation state.[10] At the same time, important differences in the Cu oxidation state were detected in TiO_2 and $BaTiO_3$ composite materials. In fact, while Cu atoms are almost totally in the Cu^{1+} state in the CuO−$BaTiO_3$ sample, CuO−TiO_2 showed a mix of Cu^{1+} and Cu^{2+} species (Figure 2b). This observation is of relevance because the reactivity (and hence the catalytic activity) of the Cu^{1+} and Cu^{2+} species can be very different.[11]

Dynamic electronic structure evolution of the catalyst surface during the photocatalytic reaction has been further investigated via *operando* NEXAFS spectroscopy. Due to the perturbation of the TEY signal during the introduction of CO_2 and H_2O, the spectra shown below were recorded in a He atmosphere at 1 bar pressure after exposure to the different reaction conditions. Moreover, NEXAFS spectra in He with and without laser illumination suggest that the laser did not impact the spectra acquisition. Prior to thermal activation, the abundance of the reduced Cu^{1+} species is higher in CuO−$BaTiO_3$ than in CuO−TiO_2, consistent with what is observed by the XPS analysis (Figure 3a−c, black spectra). However, after heating, Cu^{2+} is strongly reduced to Cu^{1+} in both samples (Figure 3a−c, red spectra). At the same time, the Ti $L_{2,3}$ edge spectra of Cu−TiO_2 show the typical features of the anatase structure, indicating an almost pure Ti^{4+} population.[20] Upon thermal treatment, we observe a small Ti^{4+}/Ti^{3+} reduction in both samples, as evidenced by the increase of the valley between the features located at ≈462.5 eV and ≈465 eV,[21] as shown in the spectra of Figure 3b−d. Moreover, the Ti L edge spectra of CuO−$BaTiO_3$ after the thermal treatment show an

https://doi.org/10.1021/acssuschemeng.5c06087
ACS Sustainable Chem. Eng. XXXX, XXX, XXX−XXX

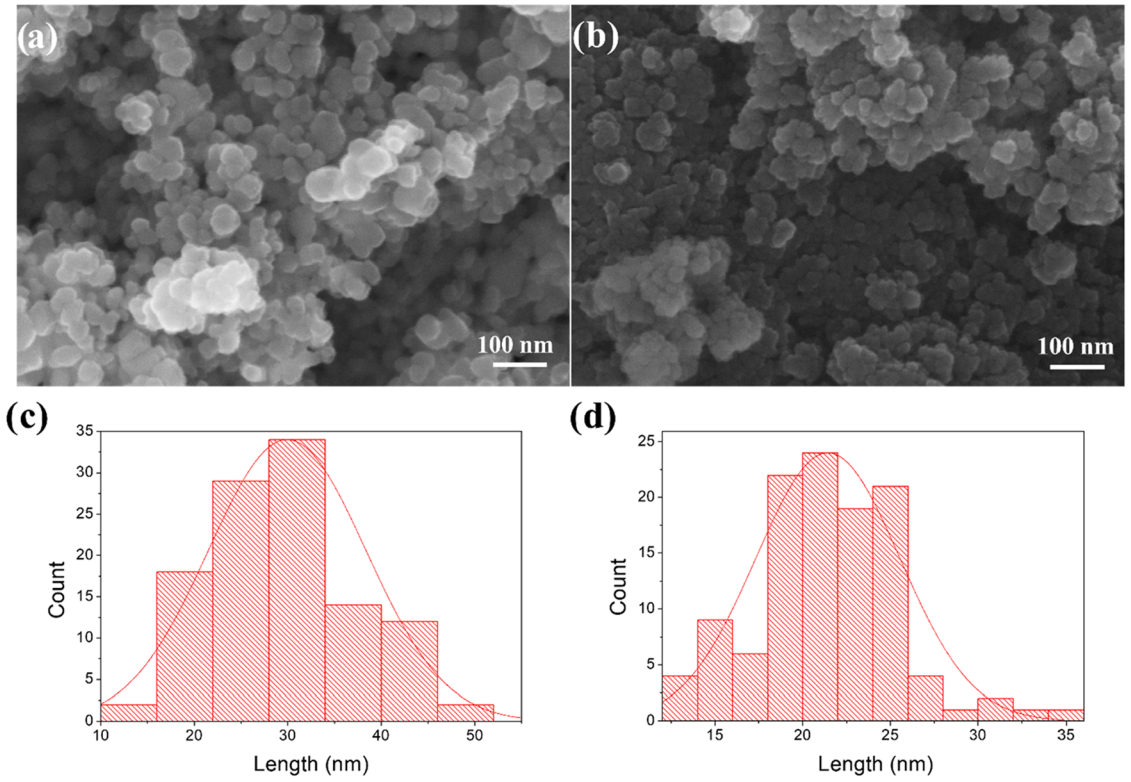

Figure 1. SEM images taken at 250k magnification showing (a) TiO_2 and (b) $BaTiO_3$ nanoparticles, with their respective size distributions (c, d).

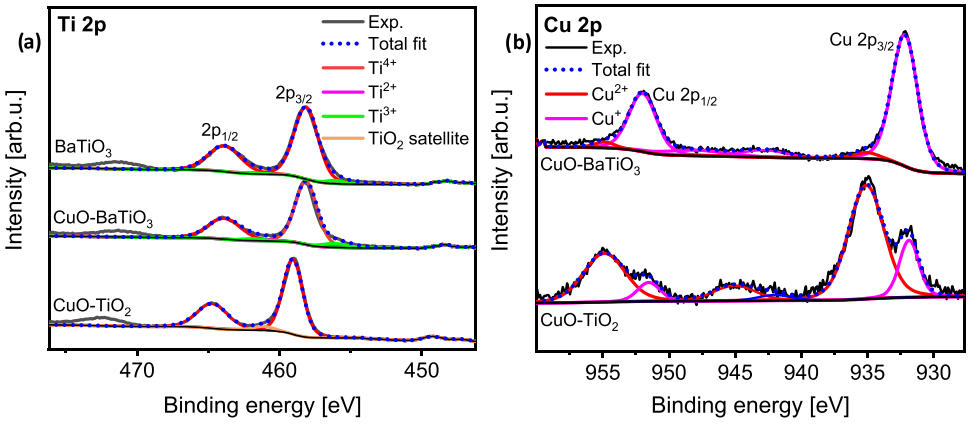

Figure 2. XPS spectra showing (a) Ti 2p core levels of $CuO-BaTiO_3$ and $CuO-TiO_2$ and (b) Cu 2p core levels collected for $CuO-BaTiO_3$ and $CuO-TiO_2$.

interesting splitting of the e_g-related feature (which was not observed in the pristine sample), which has been previously attributed to a tetragonal distortion of the $BaTiO_3$ structure as a consequence of Ti reduction.[22]

After thermal activation, the samples' reactivity toward CO_2 and H_2O in different ratios and in the presence/absence of 375 nm light illumination has been tested, and the results are shown in Figure 4. In both samples, major spectral modifications have been detected in Cu L edge spectra (Figure 4a–c), while Ti atoms have shown a relatively stable electronic structure under all the reaction conditions (Figure 4b–d). In detail, Cu absorption spectra evidenced substantial reactivity: copper was indeed totally (in $CuO-TiO_2$) or almost totally (in $CuO-BaTiO_3$) oxidized from Cu^+ to Cu^{2+} as a consequence of the interaction with the mixture of reactants. After removing CO_2 and H_2O from the sample environment and keeping a constant He (100%) flow, the initial electronic structure of Cu was gradually recovered in both samples after approximately 1 h, as shown in the light purple spectra of Figure 4a–c. This dynamic reversible behavior reveals that relatively weak bonds are formed between CuO sites and reactants/reaction intermediates, preventing surface irreversible oxidation. Changing the CO_2:H_2O ratio from 35 to 10 did not produce any spectroscopic difference on the $CuO-TiO_2$ sample, as evidenced by the bottom spectrum of Figure 4a, where it can be seen that Cu was again totally oxidized to Cu^{2+} after the 10:1 CO_2:H_2O exposure. Interestingly, in the case of $CuO-BaTiO_3$, increasing the water concentration led to the stabilization of Cu^+ sites. Figure 3c shows that a consistent amount of Cu^+ was still present on the sample surface after exposure to a 10:1 CO_2:H_2O environment.

https://doi.org/10.1021/acssuschemeng.5c06087
ACS Sustainable Chem. Eng. XXXX, XXX, XXX−XXX

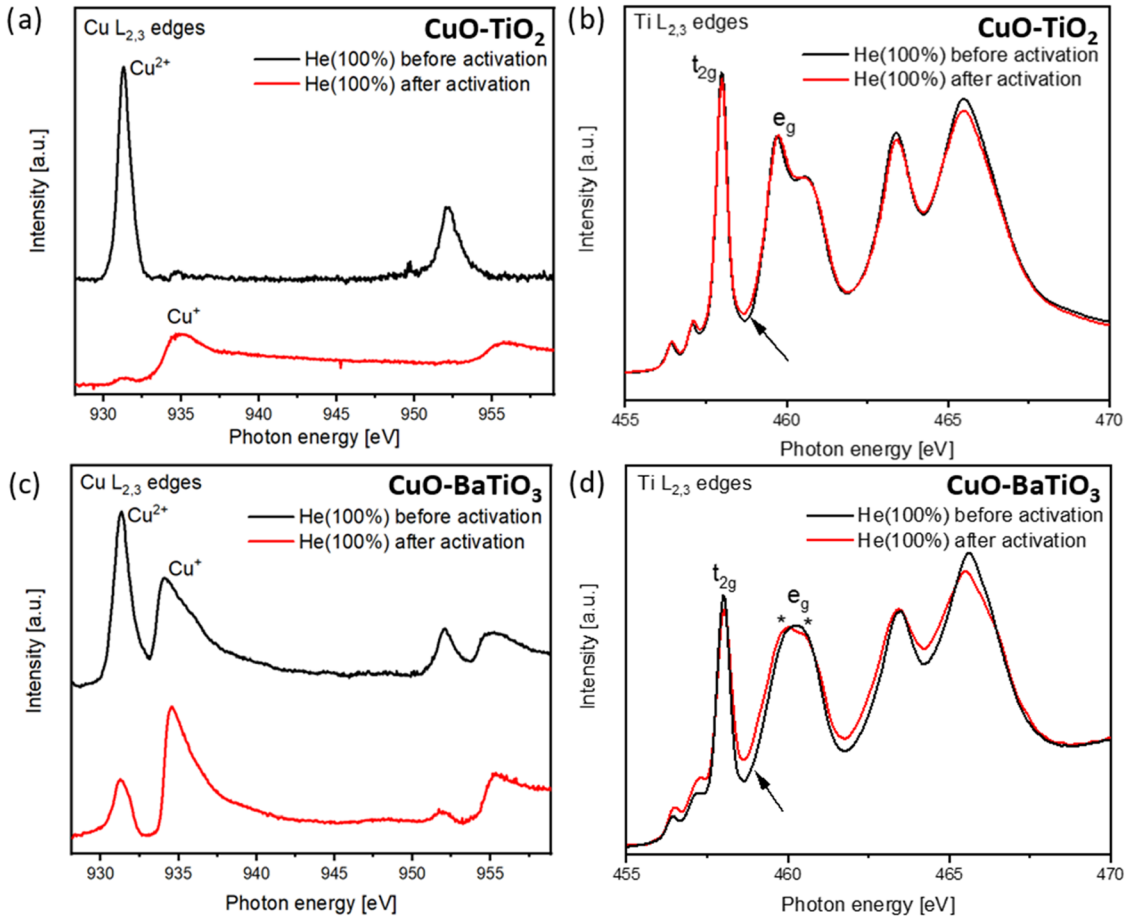

Figure 3. AP-NEXAFS spectra of the Cu $L_{2,3}$ edges for (a) CuO−TiO_2 and (c) CuO−$BaTiO_3$ and of the Ti $L_{2,3}$ edges for (b) CuO−TiO_2 and (d) CuO−$BaTiO_3$.

It was not possible to detect variations in the electronic structure at the Cu $L_{2,3}$ edges resulting from light irradiation in the presence of CO_2 and H_2O in both samples. Also, the Ti edge of the CuO−TiO_2 sample was not apparently affected by the presence of light illumination. On the other hand, a clear light-induced effect has been observed at the Ti $L_{2,3}$ edge for the CuO−$BaTiO_3$ sample. Figure 4d clearly shows that despite the Ti L_3 spectral shape being preserved under different reaction conditions, when the light is switched on, a detectable decrease in the intensity of the structure located at 462.4 eV is observed. When the light is switched off, the initial electronic structure is recovered (Figure 4d). In XAS spectroscopy, the intensity of a feature is directly proportional to the related electronic transition probability.[16] In the case of a transition metal L edge, the transition probability can be related to the occupancy of 3d orbitals; Ti^{4+} has a $3d^0$ electronic configuration nominally; thus, observing an intensity decrease of a 2p → 3d-related feature could be addressed in first approximation to an increase of the 3d occupancy. In the literature, this peak is attributed to 2p → $3dt_{2g}$ transitions.[23] Since we observed a decrease in intensity when switching on the light, it is reasonable to deduce that a photogenerated electron is filling the conduction band of Ti with electrons of d character and, in particular, of the T_{2g} orbital. Moreover, it is important to underline that this process has a lifetime long enough to be observed in the Ti L NEXAFS spectra acquired in static mode, thus indicating a strong stabilization of the photoexcited carriers in the $BaTiO_3$/CuO heterojunction. This effect has been widely reported in literature for $BaTiO_3/Cu_2O$ and TiO_2/Cu_2O p−n heterojunctions:[24−30] solar light illumination causes d−d photoexcitation of both Cu and Ti atoms, with a consequent carrier's redistribution, as depicted in Figure 5. In these types of heterojunctions, the carrier recombination process is slowed down, i.e., the lifetime of the photoexcited states is longer, with a beneficial effect on the catalytic activity.[24] In the proposed mechanism, photoexcited electrons move from the Cu to Ti conduction band, while holes move from the Ti to Cu valence bands. In order to confirm the proposed mechanism, we had to exclude that e_g filling upon light illumination could be originated by electrons photoexcited directly from Ti atoms. To this aim, we repeated the *operando* NEXAFS experiment on the bare $BaTiO_3$ sample: no Ti L edge spectra modifications upon light illumination have been observed in this case (see Figure S2): this means that in this case, the photoexcitation process is not present or the consequent charge recombination has a too short lifetime to be observed in the NEXAFS spectra.

We performed a control experiment on Ti L_3 edge spectra, switching on the light in a He(100%) flow, in order to exclude a spectroscopic modification contribution given by the reactants. Figure S3 shows that the observed spectroscopic effect persists, confirming that it is correlated with light exposure. Our experimental observation on the Ti L_3 edge of the CuO−$BaTiO_3$ material allowed us not only to directly observe the charge transfer process occurring during photoexcitation but also to identify the molecular orbitals involved in

https://doi.org/10.1021/acssuschemeng.5c06087
ACS Sustainable Chem. Eng. XXXX, XXX, XXX−XXX

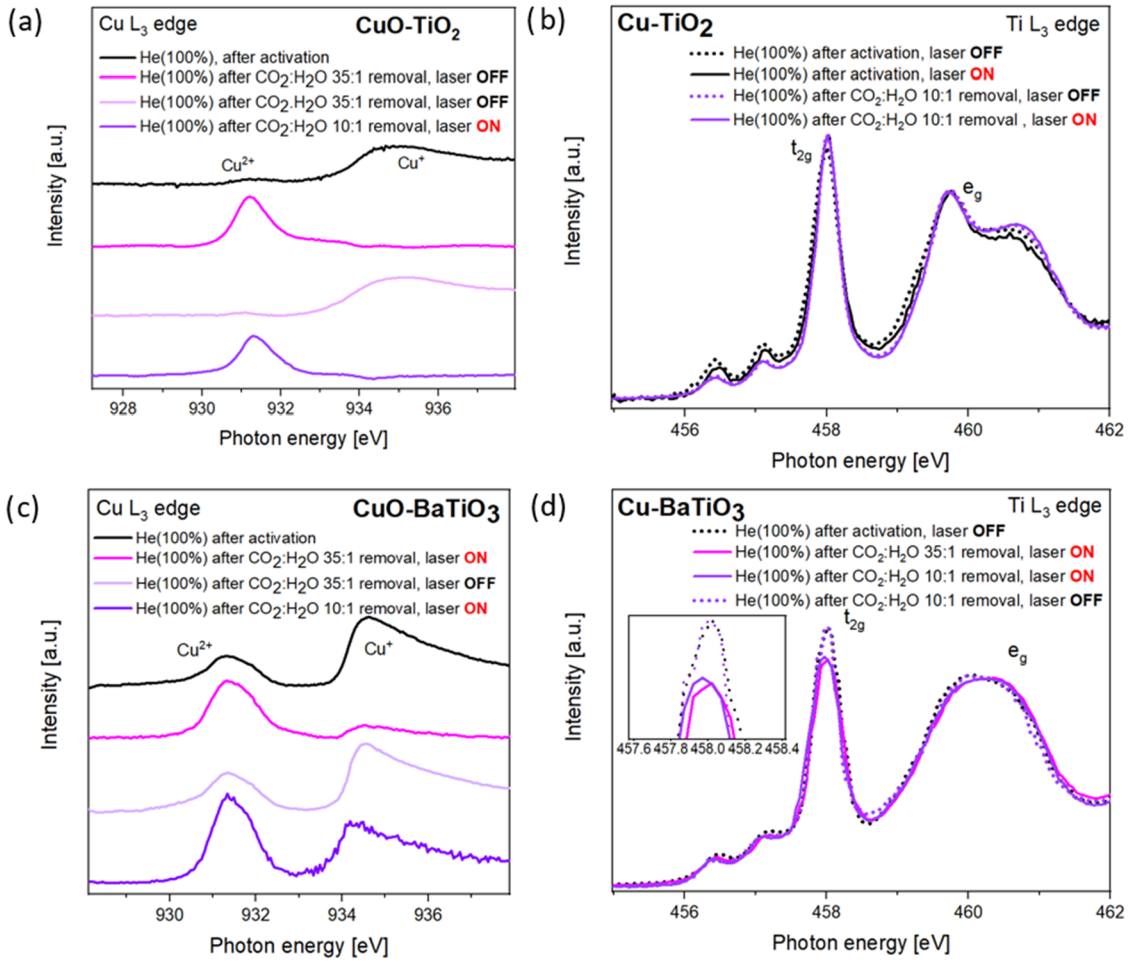

Figure 4. AP-NEXAFS of the (a–c) Cu $L_{2,3}$ edges and (b–d) Ti L_3 edge for CuO–TiO_2 and CuO–$BaTiO_3$, respectively, under different reaction conditions.

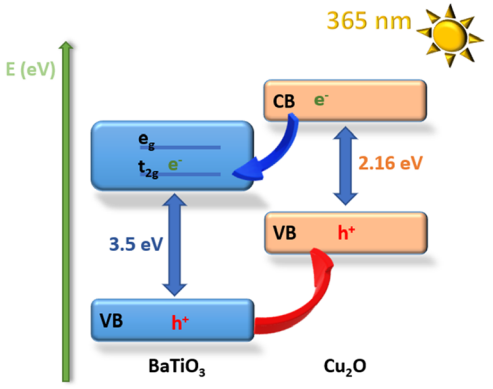

Figure 5. Proposed photoexcitation process for CuO–BaTiO, with consequent electron/hole pair redistribution. Band gap values are reported as previously observed.[10,30]

the charge separation process, i.e., t_{2g} orbitals of Ti. This effect was not observed in the CuO–TiO_2 sample, as shown in Figure 4b; in this case, we only detected a weak oxidation of Ti during the reaction with CO_2 + H_2O, as evidenced by the intensity decrease of the valley located at 463.22 eV.[21] This suggests that in the CuO–TiO_2 sample, either the excitation mechanism is different or the carrier recombination process is too fast to be observed in NEXAFS spectra.

During the whole *operando* NEXAFS experiment, we collected reaction products by micro gas chromatography, as shown in Table 2; the main observed products were CH_4 and H_2, confirming the occurrence of CO_2 and H_2O reduction reactions. From Table 2, it can be observed that (1) CH_4 is produced only by $BaTiO_3$-related samples, with CuO–$BaTiO_3$ showing a 10-fold increase in CH_4 production with respect to bare $BaTiO_3$; (2) methane is produced only when a high CO_2:H_2O ratio is used; and (3) hydrogen is produced only in CuO-containing samples.

Table 2. Gas Phase Photocatalytic Products Detected in Different Conditions after 1 h during AP-NEXAFS Analysis

sample	main reagents (ratio)	CH_4 (ppm)	H_2 (ppm)
$BaTiO_3$	CO_2 + H_2O (35:1)	0.026	0
	CO_2 + H_2O (10:1)	0	0
CuO–$BaTiO_3$	CO_2 + H_2O (35:1)	0.26	17
	CO_2 + H_2O (10:1)	0	19
CuO–TiO_2	CO_2 + H_2O (35:1)	0	19
	CO_2 + H_2O (10:1)	0	2

As well reported in the literature for CO_2 photoreduction by TiO_2, H_2 production is often favored with respect to CH_4 as a side competitive reaction, due to the affinity of Ti^{3+} for the H_2O molecule.[31] Hence, while excess H_2O enhances proton availability and promotes H_2 evolution, a higher CO_2:H_2O

https://doi.org/10.1021/acssuschemeng.5c06087
ACS Sustainable Chem. Eng. XXXX, XXX, XXX–XXX

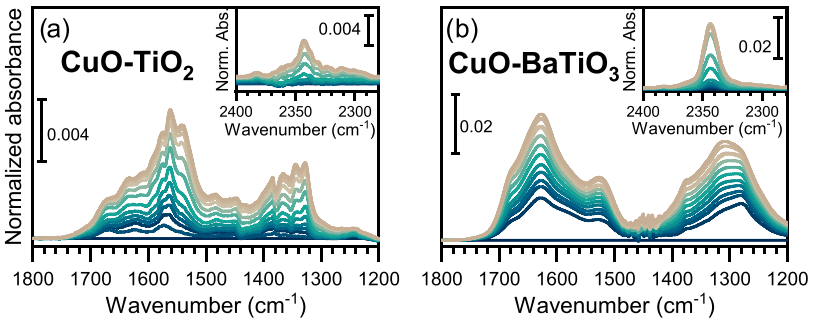

Figure 6. IR spectra of CO_2 adsorption at increasing pressures (up to 30 mbar) for the CuO−TiO_2 (a) and CuO−$BaTiO_3$ (b) samples, previously outgassed at 120 °C for 1 h. A magnification of the $\nu_{as}(CO_2)$ spectral region is reported as the inset. The spectrum of the activated material has been subtracted from all spectra.

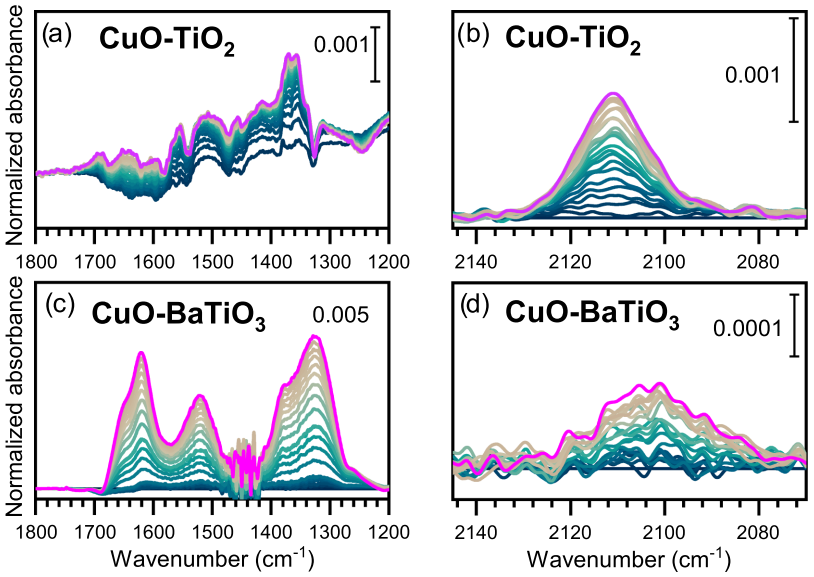

Figure 7. IR spectra at increasing time under UV irradiation of the CuO−TiO_2 (a, b) and CuO−$BaTiO_3$ (c, d) samples in the presence of CO_2 (CO_2:H_2O ratio ca. 35:1). The spectrum of the sample after the dark adsorption of CO_2 was subtracted from the entire spectral sequence.

ratio can increase the surface concentration of $CO_2^{\bullet-}$ and $HCOO^-$ intermediates, facilitating successive proton−electron transfer steps that culminate in CH_4 formation.[31,32]

Indeed, the CO_2 reduction process usually relies on the consequential transfer of 8 electrons to form CH_4, requiring electron-rich active sites able to activate the CO_2 molecule and to subsequently reduce it[33] (eq 1).

$$CO_2 + 8H^+ + 8e^- \rightarrow CH_4 + 2H_2O \quad (1)$$

For this reason, $BaTiO_3$ was indeed proposed as the material to further improve the interaction with CO_2 to favor its activation and evolution reaction, due to its natural alkalinity.[34] To validate this claim and to better understand the molecular-level interaction of CO_2 with the photocatalysts, we performed an *in situ* IR spectroscopy study on Cu−TiO_2 and Cu−$BaTiO_3$ samples. First, we investigated CO_2 adsorption in dark conditions, as shown in Figure 6. By analyzing Figure 6, at lower CO_2 pressures, we can observe the formation of bands in the spectral region between 1800 and 1200 cm^{-1}, ascribed to surface carbonates and bicarbonates. In particular, on the CuO−TiO_2 sample, we can highlight the presence of a band at 1575 cm^{-1}, assigned to monodentate carbonates, and another at 1562 cm^{-1}, attributed to bidentate bicarbonates.[35] Both spectral features are accompanied by their corresponding modes in the 1450−1300 cm^{-1} spectral region, which arise from the splitting of the doubly degenerate asymmetric stretching mode of the free carbonate, which occurs upon adsorption.[36] In the spectra of the CuO−$BaTiO_3$ sample, we can also note the presence of intense signals in the spectral region of 1700−1600 cm^{-1}, which can be attributed to the presence of both monodentate and bidentate bicarbonates.[37] Then, as the pressure increases, both samples show the growth of a band centered at 2343 cm^{-1} (see the insets in Figure 6). This signal is characteristic of linear CO_2, weakly physisorbed on the surface.[35] Finally, by also analyzing the band intensities, it is interesting to observe that the signal intensity is approximately five times higher in the CuO−$BaTiO_3$ sample compared to CuO−TiO_2, supporting the idea that the greater surface basicity of the titanate likely promoted a more effective adsorption of CO_2.

Therefore, as previously observed and as suggested by IR analysis, CO_2 interacting with the $BaTiO_3$ surface can result in the formation of $BaCO_3$ at the material's surface upon interaction with CO_2.[38] Hence, water can protonate $BaCO_3$ to form a $Ba(HCO_3)_2$ intermediate, according to eq 1, potentially favoring the consequent direct C hydrogenation.

$$BaTiO_3 + CO_2 \leftrightarrow BaCO_3 + H_2O + CO_2 \leftrightarrow Ba(HCO_3)_2 \quad (2)$$

https://doi.org/10.1021/acssuschemeng.5c06087
ACS Sustainable Chem. Eng. XXXX, XXX, XXX−XXX

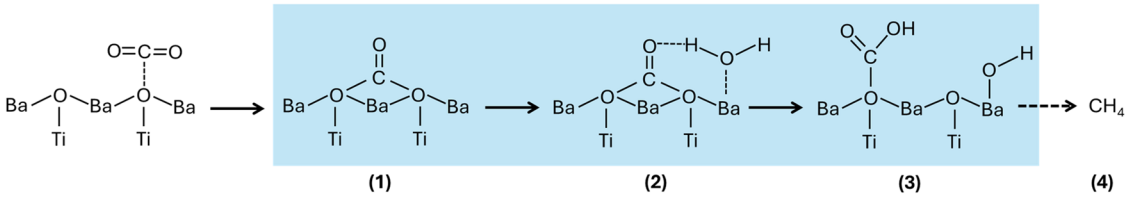

Figure 8. Proposed mechanism for methane formation on the $BaTiO_3$ surface is reported, starting from (1) the formation of bidentate carbonates and (2) bicarbonate species in the presence of water, with the consequent formation of (3) formates as starting stable intermediates for the occurrence of additional consequential reduction steps (dotted arrow), finally leading to (4) methane.

Besides, the CuO−BTO interface can promote efficient charge separation and electron trapping on Ti centers, suppressing recombination and directing electrons toward CO_2 reduction, as previously proposed[31] and as discussed below. To gain deeper insights into the surface processes occurring during the photocatalytic reaction, we performed an *in situ* IR study using a high CO_2:H_2O ratio (ca. 35:1). Figure 7 shows the measured spectra at progressively increasing UV irradiation times, following the subtraction of the last dark spectrum collected in the presence of CO_2 (see Figure 6). This procedure was applied to clearly highlight the spectral changes. Focusing on the 1800−1200 cm^{-1} spectral region (Figure 7a,c), it can be observed that the intensity of the bands formed upon irradiation is significantly higher for the CuO−$BaTiO_3$ sample. This result can be correlated with the *operando* NEXAFS measurement and online micro-GC analysis: in the same reaction conditions, we observe the photoinduced electron charge enrichment in the Ti NEXAFS spectrum of the Cu−BTO sample (Figure 4), not detected in the Cu−TiO_2 one. Moreover, micro-GC data shown in Table 2 suggest that Cu−BTO is able to produce more CH_4 than Cu−TiO_2. Combining IR, NEXAFS, and micro-GC analyses, it was possible to support the superior photoactivity of Cu−BTO. Going deeper in the reaction mechanism, among the formed reaction intermediates, we can highlight, in the CuO−TiO_2 photocatalysts, the presence of formates, which are linked to the signals around 1565 and 1360 cm^{-1}.[39] The situation is less predictable for the CuO−$BaTiO_3$ sample, in which different reaction pathways seem to coexist in parallel. Nevertheless, the formate vibrations in the 1650−1600 cm^{-1} and 1400−1300 cm^{-1} ranges are still observed, as already reported in the literature on basic oxides such as MgO.[40] Moving to the 2150−2050 cm^{-1} spectral region (Figure 7b,d), which is characteristic of the CO stretching mode, we can observe the formation of this species mainly in the CuO−TiO_2 sample. The band centered at 2110 cm^{-1} suggests that the formed CO remains adsorbed on Cu^+ sites.[41] In this regard, it was previously observed that the presence of Cu_x can improve CO adsorption[14] also potentially resulting in partial poisoning of the catalyst, thereby limiting the evolution of the reaction intermediates in the case of inefficient charge mobility and slow reaction kinetics.[42] In contrast, the adsorbed CO signal in CuO−$BaTiO_3$ is approximately an order of magnitude less intense, appearing as a broader signal shifted to lower wavenumbers, suggesting a more heterogeneous distribution of adsorption sites for the CuO particles supported on the titanate and the greater presence of Cu sites with a more metallic character.

In this case, the presence of CuO with the consequent formation of a p−n junction in CuO−$BaTiO_3$ likely resulted in the stabilization of charge carriers on the surface, enabling the regeneration and thus a higher resistance to oxidation of the Cu^+ state, as the possible consequence of the electron transfer from the n-rich to the p-depleted zone. Indeed, the XPS spectra in Figure 2 and the NEXAFS spectra in Figure 3 showed that the support-active site interaction in the Cu−BTO sample leads to a strong stabilization of active Cu^+ sites, as also supported by the IR analysis (Figure 7). This synergy with the support is also likely responsible for the slower charge recombination rate observed under UV irradiation in the NEXAFS spectra of Figure 4 for the Cu−BTO sample, which likely led to superior CO_2 evolution capabilities. Moreover, this mechanism also suggests that CO_2 activation would preferentially occur over an n-type material ($BaTiO_3$), as also supported by IR analysis, and that the presence of a p−n heterojunction can further increase the photocatalytic efficiency, as evidenced in the micro-GC results of Table 2. In bare $BaTiO_3$, the CO_2 reduction process still occurs, but with less efficiency, since in this case, the photogenerated electrons are not stabilized on t_{2g} Ti orbitals. These observations were further supported by the performed spectroscopic analysis. The NEXAFS spectra of the Ti $L_{2,3}$ edge indicated the formation of electron−hole pairs upon illumination and their slow recombination in the CuO/Cu_2O/$BaTiO_3$ system. This photoinduced electron transfer from Cu_2O/CuO to $BaTiO_3$ with slow recombination modifies the redox properties of $BaTiO_3$'s catalytically active sites, supporting a band alignment occurring at the heterojunction level. As a result, these sites become more electron-rich and are thus more capable of reducing CO_2 according to eq 1, as also previously reported.[6] In addition, the different textural properties of $BaTiO_3$-based samples may also have played a role in boosting the CH_4 production: the higher surface area of CuO−$BaTiO_3$ (137 m^2 g^{-1}) compared to CuO−TiO_2 (49 m^2 g^{-1}), along with higher average pore sizes of 13.6 and 8 nm, respectively, further favored the interaction of the reactants at the surface level, providing a higher number of active sites for the reaction to occur. Hence, in the CuO−BTO system, CH_4 formation proceeds more efficiently compared to the CuO−TiO_2 system due to the combination of the improved charge mobility resulting in more efficient reaction kinetics, peculiar textural properties, and the higher CO_2 affinity, resulting in the activation and stabilization of reaction intermediates on the $BaTiO_3$ surface. Based on the experimental evidence, the proposed pathway would lead to CH_4 starting from the formation of bicarbonate species and passing through the stabilization of formates as main reaction intermediates (Figure 8), as already observed for other catalysts.[4,43] CO_2 evolution is further improved, since Cu sites can also interact with water, participating in both water splitting and generation of protons and hydroxyl radicals and further contributing to its reduction: this proposed mechanism was supported by both the micro-GC results and the Cu L edge NEXAFS spectra of both CuO−

https://doi.org/10.1021/acssuschemeng.5c06087
ACS Sustainable Chem. Eng. XXXX, XXX, XXX−XXX

$BaTiO_3$ and $CuO-TiO_2$, where Cu^+ totally oxidizes to Cu^{2+} upon interaction with CO_2 and H_2O.

Finally, modulating the CO_2:H_2O ratio can play a role in the competitive CO_2 and H_2O reduction processes: the higher the ratio, the easier it is to produce CH_4, as already observed in our previous work.[9] Furthermore, the presence of defects such as oxygen vacancies, observed in the XPS spectra of Figure 2, can further contribute to favor the photodriven CO_2 reduction by $BaTiO_3$.[34] Therefore, the presence of defectivities in the perovskite materials can also likely influence the redox behavior of Cu. In this regard, the morphological features of the catalyst, like surface area and particle size, can have a role in modulating the availability of sites involved in the reaction. For instance, the surface area of BTO-based systems was almost 3 times higher than that of TiO_2, potentially favoring the interaction with reaction intermediates, although previous investigations found no significant contribution of the morphological properties of the catalyst to reactivity.[10]

In summary, $BaTiO_3$-based photocatalysts exhibited unique properties that can affect the selectivity of the catalytic CO_2 reduction reaction with H_2O. Although not substantially modified upon CuO addition, the higher BET surface area and the average pore size of the BTO samples may have favored the interaction with the reactants and hence the catalytic efficiency, in comparison with the TiO_2-based samples. On the other hand, the enhanced CH_4 over H_2 production, the main reaction product related to the water splitting reaction, was mainly attributed to both the higher CO_2 affinity of $BaTiO_3$ and the electronic structure modifications of both the Cu active sites and the BTO support, induced by the formation of a p−n heterojunction during the catalyst synthesis. AP-NEXAFS was exploited to explain the photocatalytic results and to enable the elucidation of the charge dynamics occurring at the heterojunction to better understand the role of Cu in the reaction. The interaction between $BaTiO_3$ and Cu can indeed enhance the stability of the most reactive Cu species and therefore the overall reactivity. Under UV light illumination, photoexcited electrons move from Cu sites to the t_{2g} empty orbitals of Ti sites, enabling a slow charge recombination that can boost the CO_2 reduction mechanism. This behavior is not observed when a different support ($CuO-TiO_2$) is used, revealing a unique metal−support interaction of CuO−BTO. CH_4 production in CuO−BTO proceeds through CO_2 activation and the consequent formation of carbonates. H_2O, activated by Cu sites, contributes in further reducing carbonates, eventually leading to the desorption of methane through the intermediate formation of formates.

CONCLUSIONS

In this work, we report the results of a combination of complementary spectroscopic techniques (*operando* NEXAFS at ambient pressure and *in situ* IR) to investigate the reactivity of CuO NPs supported by two different Ti-based oxides, namely, CuO−BTO and $CuO-TiO_2$, during the CO_2 photoreduction reaction with H_2O. The measurements enabled us to conclude that the methanation reaction is enhanced in the $CuO-BaTiO_3$ system with respect to the $CuO-TiO_2$ counterpart and that the activity and selectivity of both catalysts are tuned by the presence of a reversible redox couple Cu^+/Cu^{2+} in the CuO NPs. The NEXAFS analysis performed during UV light irradiation enabled for the first time direct localization of the photoexcited electrons in the CuO−BTO sample in the t_{2g} 3d orbitals of Ti sites, thus demonstrating the longer lifetime of the photoexcited state in CuO−BTO with respect to the $CuO-TiO_2$ sample. This process is mainly responsible for the different redox behaviors observed between the CuO−BTO and the $CuO-TiO_2$ samples and for the enhanced methanation capabilities of the Cu−BTO sample. In fact, $BaTiO_3$ may enhance resistance to Cu oxidation via n → p electron flow, thereby favoring the regeneration of the active species for the photocatalytic reaction. Moreover, the electron enrichment of Ti sites under illumination caused by the photoexcitation process favors the CO_2 reduction reaction. Additionally, $BaTiO_3$ properties such as the high BET surface area and high CO_2 affinity further contributed to boosting CH_4 production. The combined spectroscopic and gas product analysis during the reaction enabled the formulation of a possible reaction mechanism, involving the activation of CO_2 in the form of carbonates and bicarbonates, and their further reduction to CH_4 molecules through the formation of formates as intermediates, favored by the unique photoinduced electronic properties of the Cu−BTO catalyst. This study shows how perovskite-based supported catalysts can induce the formation of heterojunctions that are extremely functional to the charge recombination suppression in photoinduced catalytic processes. The detailed experimental exploration of the photoexcitation process in these types of materials, carried out exploiting forefront *operando* spectroscopic techniques, can pave the way for the design of more efficient photocatalysts for valuable hydrocarbon production.

EXPERIMENTAL METHODS

Material Preparation

The photocatalysts were prepared via hydrothermal synthesis, as previously described.[11] Briefly, copper oxide nanoparticles (CuO NPs) were synthesized by dissolving 2.0 g of $CuSO_4 \cdot 5H_2O$ into 50 mL of Milli-Q H_2O in a beaker while stirring at 900 rpm for 30 min. Therefore, the pH was set at 8.5 by adding 4 M NaOH (Sigma-Aldrich, ≥ 98%) dropwise. The solution was left under stirring at 1000 rpm for 3 h. Therefore, the mixture was treated in an autoclave at 180 °C for 18 h. After hydrothermal treatment, the obtained precipitate was filtered, washed with Milli-Q water and ethanol, and dried at 110 °C for 18 h. The sample was then calcinated at 300 °C for 3 h in the presence of N_2. Barium titanate ($BaTiO_3$) was synthesized by a modified solvothermal process, by pouring 50 mL of a 0.1 M $BaCl_2$ solution (Fluka Analytical) and titanium(IV) isopropoxide (Sigma-Aldrich, 97%) in a beaker in a 1:1 molar ratio. The pH was adjusted to 12 with 4 M NaOH (Sigma-Aldrich, ≥98%). The solution was left under stirring for 1 h and then treated hydrothermally at 180 °C for 8 h. The sample was filtered, washed, and dried at 110 °C for 18 h. P25 (Evonik) was used as a benchmark material for TiO_2-based catalysts. Therefore, $CuO-BaTiO_3$ and $CuO-TiO_2$ were obtained via incipient wetness impregnation, by decorating either $BaTiO_3$ or TiO_2, respectively, with 2.5 wt % CuO NPs previously synthesized. The defined corresponding amount of CuO was dispersed in 1 mL of ethanol, sonicated for 30 min, and then used to impregnate the support material. The materials were then dried for 18 h at 110 °C

Structural Characterization

N_2 physisorption was carried out with a Tristar II Plus Micrometrics (Micromeritics), by treating 100 mg of each catalyst in vacuum for 2 h, at room temperature in the case of $BaTiO_3$ and $CuO-BaTiO_3$ and at 200 °C in the case of $CuO-TiO_2$, as Ba-based materials had not been calcinated. Specific surface area was determined according to the Brunauer−Emmet−Teller (BET) theory.[36] Scanning electron microscopy (SEM) and energy-dispersive X-ray spectroscopy (EDS) were

https://doi.org/10.1021/acssuschemeng.5c06087
ACS Sustainable Chem. Eng. XXXX, XXX, XXX−XXX

performed with a Crossbeam 550 (Zeiss), as previously reported[1111] A small quantity of specimens was collected into a vial and dispersed in 1 mL of ethanol. The solution was sonicated for 30 min and then loaded on a silicon wafer. The wafer was deposited on a steel stub and anchored with a thin copper wire string, which also has the role of enhancing the sample conductivity.

Spectroscopic Characterization

X-ray photoelectron spectroscopy (XPS) experiments were performed at the laboratories of the Advanced Photoelectric Effect−High Energy (APE-HE) beamline at Elettra Synchrotron in Trieste, Italy, exploiting a conventional non-monochromatized X-ray source (Al Kα = 1486 eV) with a hemispherical electron energy analyzer.[37] The powders were glued on the sample holder using a conductive silver paste. The samples have been positioned at 45° with respect to the incident beam, probing an area of ∼1 mm^2 and a depth of ∼1 nm. The Ti 2p and Cu 2p XPS spectra were acquired using a pass energy of 50 and a dwell time of 1000 ms; they were aligned using the Au VB spectra of a reference Au foil positioned just above the sample. The data analysis (including the energy alignment and fitting process) has been performed using Origin (OriginLab Corporation, Northampton, MA, USA) and CasaXPS software.[38] For the fitting process, asymmetric Lorentzian line shape functions have been employed.

Ambient-pressure near-edge X-ray absorption spectra (AP-NEXAFS) were measured at the APE-HE beamline of the Elettra Italian Synchrotron radiation source. The catalysts to be investigated were placed individually in a custom-designed reactor cell (Figure 1a,b), which has been mounted on a dedicated UHV chamber.[39] Exploiting a Si_3N_4 membrane, the chemical reactor containing the sample stays at 1 bar total pressure, while the synchrotron soft X-rays can interact with the catalyst surface to give the absorption signal. The total electron yield (TEY) mode was used to record the experimental spectra, having a surface sensitivity of ≈5 nm. Cu L_3 edge spectra were collected from 880 to 950 eV, while Ti $L_{2,3}$ edges were collected from 450 to 480 eV. The catalysts were first subjected to a thermal activation treatment at 120 °C for 1 h at atmospheric pressure of helium. After the treatment, the catalysts were cooled to room temperature, and afterward, they were exposed to the reagents (CO_2 + H_2O) with two different ratios (10:1 and 35:1) exploiting an external gas line (Figure S1, panel c) in either dark or irradiation for 1 h with UV light (365 nm), with the NEXAFS spectra being continuously recorded. The gas reaction products were detected with a combined micro-GC and mass spectrometry system (Figure S1, panel d). As shown in Figure S1, the detection systems are directly connected to the outlet of the gas line. To avoid the condensation of the products in the line, the injector of the micro-GC is heated to 90 °C. Spectra were background-subtracted, and energy was aligned with Origin software. The Cu^+/Cu^{2+} spectral components were tracked in the presence of different reagents, both in dark and UV-irradiated conditions.

Fourier transform Infrared (FTIR) spectroscopic measurements were performed in transmission mode at a resolution of 2 cm^{-1} by using a Bruker INVENIO FTIR spectrometer equipped with an MCT detector. Each spectrum was obtained by averaging 128 individual scans. Samples were pressed into self-supporting pellets (optical density of ca. 13 mg·cm^{-2}) and placed in a customized quartz IR cell equipped with KBr windows, allowing in situ experiments.

Before measurement, each material was heated under a dynamic vacuum from room temperature up to 150 °C and maintained at this temperature for 1 h, reaching a residual pressure of 5 × 10^{-4} mbar. The sample was then cooled to room temperature, and after collecting the IR spectrum of the activated sample, CO_2 was introduced stepwise into the cell up to a final pressure of 30 mbar. The system was kept in the dark for 30 min at the final pressure, until no further spectral changes were observed.

Subsequently, the photocatalysts were irradiated with UV light for approximately 2 h using a Newport 500 W Hg (Xe) arc lamp. A water filter was used to remove the IR component, and a large-core liquid light guide was employed to focus the beam onto the pellet inside the in situ cell. During irradiation, IR spectra were collected sequentially: 5 spectra with a 1 s interval, 5 spectra with a 5 min interval, and 10 spectra with a 10 min interval. The spectra were normalized to the optical density of the pellets.

ASSOCIATED CONTENT

Supporting Information

The Supporting Information is available free of charge at https://pubs.acs.org/doi/10.1021/acssuschemeng.5c06087.

Custom-made operando soft-NEXAFS setup (Figure S1); AP-NEXAFS spectra of Ti $L_{2,3}$ edges in $BaTiO_3$ (Figure S2); and NEXAFS spectra of Ti $L_{2,3}$ edges in CuO−$BaTiO_3$ in laser ON/OFF conditions (Figure S3) (PDF)

AUTHOR INFORMATION

Corresponding Author

Silvia Mauri − *CNR—Istituto Officina dei Materiali, TASC, I-34149 Trieste, Italy;* orcid.org/0000-0003-2183-4293; Email: mauri@iom.cnr.it

Authors

Giulia Forghieri − *Department of Molecular Sciences and Nanosystems, Ca' Foscari University and INSTM RU of Venice, 30172 Venice, Italy*

Sara Stolfi − *CNR—Istituto Officina dei Materiali, TASC, I-34149 Trieste, Italy; Department of Chemistry, University of Pavia, I-27100 Pavia, Italy*

Elena Ghedini − *Department of Chemistry, University of Bari Aldo Moro, 70121 Bari, Italy*

Elizaveta Kozyr − *Department of Chemistry and Interdepartmental NIS Centre, University of Torino, 10125 Torino, Italy*

Lorenzo Mino − *Department of Chemistry and Interdepartmental NIS Centre, University of Torino, 10125 Torino, Italy;* orcid.org/0000-0002-9882-8361

Piero Torelli − *CNR—Istituto Officina dei Materiali, TASC, I-34149 Trieste, Italy*

Michela Signoretto − *Department of Molecular Sciences and Nanosystems, Ca' Foscari University and INSTM RU of Venice, 30172 Venice, Italy;* orcid.org/0000-0002-0051-2968

Complete contact information is available at: https://pubs.acs.org/10.1021/acssuschemeng.5c06087

Notes

The authors declare no competing financial interest.

ACKNOWLEDGMENTS

This work was partly performed in the framework of the nanoscience foundry and fine analysis (NFFA-MIUR Italy Progetti Internazionali) project. The results were partly accomplished within the SCORE2 project funded by PRIN 2022 PNRR.

REFERENCES

(1) Bai, Y.; Barau, A. S.; Diouf, A. A.; Janz, B.; Manning, F.; Contreras, E. M.; Nampanzira, D.; Ng, C. C.; Paulos, H. B.; Xu, X.; Zichali, T. Technical Summary. In *Climate Change and Land: an IPCC Special Report On Climate Change, Desertification, Land Degradation, Sustainable Land Management, Food Security, And Greenhouse Gas Fluxes In Terrestrial Ecosystems*; Shukla, P.; Skea, J.; Slade, R.; van

Diemen, R.; Haughey, E.; Malley, J.; Pathak, M.; Pereira Portugal, J., Eds.; Cambridge University Press, 2022; pp 37−74.
(2) Yuan, Y.; You, H.; Ricardez-Sandoval, L. Recent Advances on First-Principles Modeling for the Design of Materials in CO_2 Capture Technologies. *Chin. J. Chem. Eng.* **2019**, *27*, 1554−1565.
(3) Zhou, H.; Wang, J.; Meng, W.; Wang, K.; Li, G.; Yang, Y.; Fan, Z.; Wang, D.; Ji, D. Comparative Investigation of CO_2-to-Methanol Process Using Different CO_2 Capture Technologies. *Fuel* **2023**, *338*, No. 127359.
(4) Thompson, W. A.; Fernandez, E. S.; Maroto-Valer, M. M. Review and Analysis of CO_2 Photoreduction Kinetics. *ACS Sustainable Chem. Eng.* **2020**, *8* (12), 4677−4692.
(5) Vasileff, A.; Xu, C.; Jiao, Y.; Zheng, Y.; Qiao, S. Z. Surface and Interface Engineering in Copper-Based Bimetallic Materials for Selective CO_2 Electroreduction. *Chem* **2018**, *4*, 1809−1831.
(6) Kumar Sahoo, S.; P, A.; Ray, K.; Pandey, D. Addition of CuO to Form CuO/TiO_2 and CuO/ZnO Heterojunctions for Photocatalytic CO_2 Conversion to Methanol. *Chem. Phys. Lett.* **2024**, *856*, No. 141678.
(7) Karthik, K. V.; Reddy, C. V.; Reddy, K. R.; Ravishankar, R.; Sanjeev, G.; Kulkarni, R. V.; Shetti, N. P.; Raghu, A. V. Barium Titanate Nanostructures for Photocatalytic Hydrogen Generation and Photodegradation of Chemical Pollutants. *J. Mater. Sci.: Mater. Electron.* **2019**, *30* (23), 20646−20653.
(8) Lee, W. W.; Chung, W. H.; Huang, W. S.; Lin, W. C.; Lin, W. Y.; Jiang, Y. R.; Chen, C. C. Photocatalytic Activity and Mechanism of Nano-Cubic Barium Titanate Prepared by a Hydrothermal Method. *J. Taiwan Inst. Chem. Eng.* **2013**, *44* (4), 660−669.
(9) Ferraro, G.; Di Vera, A.; Ghedini, E.; Marchiori, M.; Forghieri, G.; Canton, P.; Signoretto, M. Carbon-Dots-Conjugated Semiconductors for Enhanced Solar-Driven Photocatalysis. *Appl. Catal., O: Open* **2024**, *192*, No. 206942.
(10) Virdee, A. K.; Martin, I.; Tan, J. Z. Y.; Forghieri, G.; Maroto-Valer, M. M.; Signoretto, M.; Van der Spek, M.; Andresen, J. M. Investigation of Process Parameters for Solar Fuel Production Using Earth-Abundant Materials. *J. CO2 Util.* **2023**, *75*, No. 102568.
(11) Nogueira, A. E.; Oliveira, J. A.; da Silva, G. T. S. T.; Ribeiro, C. Insights into the Role of CuO in the CO_2 Photoreduction Process. *Sci. Rep* **2019**, *9* (1), No. 1316.
(12) Nogueira, A. E.; da Silva, G. T. S. T.; Oliveira, J. A.; Torres, J. A.; da Silva, M. G. S.; Carmo, M.; Ribeiro, C. Unveiling CuO Role in CO_2 Photoreduction Process − Catalyst or Reactant? *Catal. Commun.* **2020**, *137*, No. 105929.
(13) Wan, L.; Zhou, Q.; Wang, X.; Wood, T. E.; Wang, L.; Duchesne, P. N.; Guo, J.; Yan, X.; Xia, M.; Li, Y. F.; Ali, F. M.; Ulmer, U.; Jia, J.; Li, T.; Sun, W.; Ozin, G. A. Cu_2O Nanocubes with Mixed Oxidation-State Facets for (Photo)Catalytic Hydrogenation of Carbon Dioxide. *Nat. Catal* **2019**, *2* (10), 889−898.
(14) Deng, Z.; Hu, S.; Ji, J.; Wu, S.; Xie, H.; Xing, M.; Zhang, J. Deep Insight of the Influence of Cu Valence States in Co-Catalyst on CO_2 Photoreduction. *Appl. Catal., B* **2022**, *316*, No. 121621.
(15) Wang, W.; Deng, C.; Xie, S.; Li, Y.; Zhang, W.; Sheng, H.; Chen, C.; Zhao, J. Photocatalytic C-C Coupling from Carbon Dioxide Reduction on Copper Oxide with Mixed-Valence Copper(I)/Copper(II). *J. Am. Chem. Soc.* **2021**, *143* (7), 2984−2993.
(16) Joachim, S. *NEXAFS Spectroscopy*, 1st ed.; Springer: Berlin, Heidelberg, 1992.
(17) Vikatakavi, A.; Mauri, S.; Rivera-Salazar, M. L.; Dobovičnik, E.; Pelatti, S.; D'Addato, S.; Torelli, P.; Luches, P.; Benedetti, S. Role of Metal Dopants in Hydrogen Dissociation on $Cu:CeO_2$ and $Fe:CeO_2$ Surfaces Studied by Ambient-Pressure X-Ray Absorption Spectroscopy. *ACS Appl. Energy Mater.* **2024**, *7* (7), 2746−2754.
(18) Mauri, S.; Calligaro, R.; Pauletti, C. F.; Camellone, M. F.; Boaro, M.; Braglia, L.; Fabris, S.; Piccinin, S.; Torelli, P.; Trovarelli, A. Low-Temperature Methane Activation Reaction Pathways over Mechanochemically-Generated Ce^{4+}/Cu^{+} Interfacial Sites. *Small* **2024**, *20*, No. 2403028.
(19) Braglia, L.; Tavani, F.; Mauri, S.; Edla, R.; Krizmancic, D.; Tofoni, A.; Colombo, V.; D'Angelo, P.; Torelli, P. Catching the Reversible Formation and Reactivity of Surface Defective Sites in Metal-Organic Frameworks: An Operando Ambient Pressure-NEXAFS Investigation. *J. Phys. Chem. Lett.* **2021**, *12* (37), 9182−9187.
(20) Bittencourt, C.; Krüger, P.; Lagos, M. J.; Ke, X.; Van Tendeloo, G.; Ewels, C.; Umek, P.; Guttmann, P. Towards Atomic Resolution in Sodium Titanate Nanotubes Using Near-Edge X-Ray-Absorption Fine-Structure Spectromicroscopy Combined with Multichannel Multiple-Scattering Calculations. *Beilstein J. Nanotechnol.* **2012**, *3* (1), 789−797.
(21) Bassato, F.; Mauri, S.; Braglia, L.; Petrov, A. Y.; Dobovičnik, E.; Tavani, F.; Tofoni, A.; Ferrer, P.; Grinter, D.; Held, G.; D'Angelo, P.; Torelli, P. $La_{0.2}Sr_{0.25}Ca_{0.45}TiO_3$ Surface Reactivity with H_2: A Combined Operando NEXAFS and Computational Study. *J. Phys. Chem. Lett.* **2024**, *15* (33), 8540−8548.
(22) Zhang, W.; Feng, Q.; Hosono, E.; Asakura, D.; Miyawaki, J.; Harada, Y. Tetragonal Distortion of a $BaTiO_3/Bi_{0.5}Na_{0.5}TiO_3$ nanocomposite Responsible for Anomalous Piezoelectric and Ferroelectric Behaviors. *ACS Omega* **2020**, *5* (36), 22800−22807.
(23) De Groot, F. M. F.; Fuggle, J. C.; Thole, B. T.; Sawatzky, G. A. L q 3 X-Ray-Absorption Edges of d Compounds: K+, Ca2+, Sc'+, and Ti+ in Oh (Octahedral) Symmetry. *Phys. Rev. B* **1990**, *41*, No. 928.
(24) Li, C.; Fang, T.; Hu, H.; Wang, Y.; Liu, X.; Zhou, S.; Fu, J.; Wang, W. Synthesis and Enhanced Bias-Free Photoelectrochemical Water-Splitting Activity of Ferroelectric $BaTiO_3/Cu_2O$ Heterostructures under Solar Light Irradiation. *Ceram. Int.* **2021**, *47* (8), 11379−11386.
(25) Xiao, L.; Tian, F.; Lu, P.; Zhang, F.; Zhang, Y.; Zhang, Q.; Hu, Z.; Xiong, J. Enhanced Piezo-Photocatalytic Performance of $Cu_2O/BaTiO_3$ p−n Heterojunction for Efficient Dye Degradation. *J. Mater. Sci.* **2025**, *60* (9), 4279−4292.
(26) Joshi, S.; Ippolito, S. J.; Periasamy, S.; Sabri, Y. M.; Sunkara, M. V. Efficient Heterostructures of $Ag@CuO/BaTiO_3$ for Low-Temperature CO_2 Gas Detection: Assessing the Role of Nanointerfaces during Sensing by Operando DRIFTS Technique. *ACS Appl. Mater. Interfaces* **2017**, *9* (32), 27014−27026.
(27) Sharma, D.; Upadhyay, S.; Satsangi, V. R.; Shrivastav, R.; Waghmare, U. V.; Dass, S. Nanostructured $BaTiO_3/Cu_2O$ Heterojunction with Improved Photoelectrochemical Activity for H_2 Evolution: Experimental and First-Principles Analysis. *Appl. Catal., B* **2016**, *189*, 75−85.
(28) Xu, H.; Ouyang, S.; Liu, L.; Wang, D.; Kako, T.; Ye, J. Porous-Structured Cu_2O/TiO_2 Nanojunction Material toward Efficient CO_2 Photoreduction. *Nanotechnology* **2014**, *25* (16), No. 165402.
(29) Bessekhouad, Y.; Robert, D.; Weber, J. V. Photocatalytic Activity of Cu_2O/TiO_2, Bi $_2O_3/TiO_2$ and $ZnMn_2O_4/TiO_2$ Heterojunctions. *Catal. Today* **2005**, *101*, 315−321.
(30) Heinemann, M.; Eifert, B.; Heiliger, C. Band Structure and Phase Stability of the Copper Oxides Cu_2O, CuO, and Cu_4O_3. *Phys. Rev. B* **2013**, *87* (11), No. 115111.
(31) Ibarra-Rodriguez, L. I.; Pantoja-Espinoza, J. C.; Luévano-Hipólito, E.; Garay-Rodríguez, L. F.; López-Ortiz, A.; Torres-Martínez, L. M.; Collins-Martínez, V. H. Formic Acid and Hydrogen Generation from the Photocatalytic Reduction of CO_2 on Visible Light Activated $N\text{-}TiO_2/CeO_2/CuO$ Composites. *J. Photochem., Photobiol.* **2022**, *11*, No. 100125.
(32) Olivo, A.; Thompson, W. A.; Bay, E. R. B.; Ghedini, E.; Menegazzo, F.; Maroto-Valer, M.; Signoretto, M. Investigation of Process Parameters Assessment via Design of Experiments for CO_2 Photoreduction in Two Photoreactors. *J. CO2 Util.* **2020**, *36*, 25−32.
(33) Wang, P.; Yang, F.; Qu, J.; Cai, Y.; Yang, X.; Li, C. M.; Hu, J. Recent Advances and Challenges in Efficient Selective Photocatalytic CO_2 Methanation. *Small* **2024**, *20*, No. 2400700.
(34) Dasireddy, V. D. B. C.; Likozar, B. Photocatalytic CO_2 Reduction to Methanol over Bismuth Promoted BaTiO3 Perovskite Nanoparticle Catalysts. *Renewable Energy* **2022**, *195*, 885−895.
(35) Mino, L.; Spoto, G.; Ferrari, A. M. CO_2 Capture by TiO_2 Anatase Surfaces: A Combined DFT and FTIR Study. *J. Phys. Chem. C* **2014**, *118* (43), 25016−25026.

https://doi.org/10.1021/acssuschemeng.5c06087
ACS Sustainable Chem. Eng. XXXX, XXX, XXX−XXX

(36) Busca, G.; Lorenzelli, V. Infrared Spectroscopic Identification of Species Arising from Reactive Adsorption of Carbon Oxides on MetalOxides. *Mater. Chem.* **1982**, *7*, 89−126.
(37) Mino, L.; Cesano, F.; Scarano, D.; Spoto, G.; Martra, G. Molecules and Heterostructures at TiO_2 Surface: The Cases of H_2O, CO_2, and Organic and Inorganic Sensitizers. *Res. Chem. Intermed.* **2019**, *45*, 5801−5829.
(38) Herrán, J.; Mandayo, G. G.; Castaño, E. Physical Behaviour of $BaTiO_3$-CuO Thin-Film under Carbon Dioxide Atmospheres. *Sens. Actuators, B* **2007**, *127*, 370−375.
(39) Sun, S.; Ding, J.; Bao, J.; Gao, C.; Qi, Z.; Li, C. Photocatalytic Oxidation of Gaseous Formaldehyde on TiO_2: An in Situ DRIFTS Study. *Catal. Lett.* **2010**, *137*, 239−246.
(40) Busca, G.; Lamotte, J.; Lavalley, J.-C.; Lorenzelli, V. FT-IR Study of the Adsorption and Transformation of Formaldehyde on Oxide Surfaces. *J. Am. Chem. Soc.* **1987**, *109*, 5197−5202.
(41) Escolano Casado, G.; Ivanchenko, P.; Paul, G.; Bisio, C.; Marchese, L.; Ashrafi, A. M.; Milosavljevic, V.; Degli Esposti, L.; Iafisco, M.; Mino, L. Surface and Structural Characterization of Cu-Exchanged Hydroxyapatites and Their Application in H_2O_2 Electrocatalytic Reduction. *Appl. Surf. Sci.* **2022**, *595*, No. 153495.
(42) Liu, Y.; Zhou, Y. Synergistic Mechanisms of Dual-Metal Single-Atoms Catalysts for Promoting CO_2 Photoreduction: Bifunctional, Intersite Distance, and Electronic Effects. *ACS Catal.* **2025**, *15* (13), 10957−10970.
(43) Wang, Y.; Chen, E.; Tang, J. Insight on Reaction Pathways of Photocatalytic CO_2 Conversion. *ACS Catal.* **2022**, *12*, 7300−7316.

https://doi.org/10.1021/acssuschemeng.5c06087
ACS Sustainable Chem. Eng. XXXX, XXX, XXX−XXX